Kinetic Monte Carlo simulation of escaping core plasma particles to the scrape-off layer for accurate response of plasma-facing components

2013 Nucl. Fusion 53 073023

(http://iopscience.iop.org/0029-5515/53/7/073023)

Nucl. Fusion **53** (2013) 073023 (8pp) doi:10.1088/0029-5515/53/7/073023

Kinetic Monte Carlo simulation of escaping core plasma particles to the scrape-off layer for accurate response of plasma-facing components

V. Sizyuk and A. Hassanein

Center for Materials under Extreme Environment, School of Nuclear Engineering, Purdue University, West Lafayette 47907, USA

E-mail: vsizyuk@purdue.edu (V. Sizyuk) and hassanein@purdue.edu (A. Hassanein)

Received 15 October 2012, accepted for publication 13 May 2013
Published 11 June 2013
Online at stacks.iop.org/NF/53/073023

Abstract
During normal and disruptive operations in tokamak devices the escaped core plasma particles are a potential threat to the divertor and nearby component lifetime as well as plasma contamination. Comprehensive enhanced physical and numerical models are developed and implemented in the upgraded High Energy Interaction with General Heterogeneous Target Systems (HEIGHTS) package to accurately predict the impact of the escaped particles on plasma-facing and nearby components. An *ab initio* Monte Carlo-based kinetic model of the escaping core particles is developed for integration with the magnetohydrodynamic (MHD) models of the initiated edge plasma where the escaping particles are used as an input volume source. The paper describes details of the 3D Monte Carlo kinetic model, validation and benchmarking and simulation results for both National Spherical Torus Experiment and ITER devices using actual reactor design and magnetic configurations. The simulation results are being implemented self-consistently with various HEIGHTS models that include surface erosion, divertor plasma generation, plasma MHD evolution, heat conduction and detailed photon transport of line and continuum radiation.

1. Introduction

Successful development of future fusion reactors critically depends on the correct prediction of the heat and particle loads to reactor walls and the optimum material choice for plasma-facing components (PFCs). Experimental data of current tokamak devices and theoretical predictions show that future ITER-like surfaces should be resistant both to steady-state heat flux of up to 20 MW m^{-2} and to intense transient (τ = 0.1–10 ms) events of up to 10 GW m^{-2}. The divertor plate is a key component of the tokamak device. High particle and heat fluxes can cause high surface sputtering, melt and vaporization erosion, plasma contamination and component failure that can interrupt normal operation of the reactor. The reactor geometry, the magnetic configuration and the interaction processes in the scrape-off layer (SOL) determine not only heat transport and loads to component surfaces but also play an important role in plasma confinement and control the transition to the high-confinement mode (H-mode) operation. Experiments in current tokamak devices show the complex behaviour of edge plasma interaction with device components and as a result the required understanding of the complex self-consistent behaviour of plasma in the entire SOL configuration. The edge plasma interaction with component surfaces affects the behaviour of deuterium–tritium (DT) bulk plasma and impurity contaminations, influences toroidal plasma motion and redistributes energy loads among reactor components. Damage of plasma-facing and structural materials due to loss of plasma confinement remains one of the most serious concerns for safe, successful and reliable reactor operation. Plasma instabilities occur in various forms such as hard disruptions, which include both thermal and current quench, edge-localized modes (ELMs), runaway electrons and vertical displacement events (VDEs). Therefore, accurate understanding of the escaping core plasma into SOL and the subsequent interaction with device components is extremely important for successful development, operation and optimization of future fusion devices. Current fusion reactors have complex 3D design and simple one- or two-dimensional models cannot be used for correct description of self-consistent processes of edge plasma evolution. Transport of charged particles in tokamak plasma environment is best described by kinetic theory [1]. However, solving the full kinetic equations remains an impractical task and most recent

investigations [2–5] are based on the magnetohydrodynamic (MHD) approach for modelling the core plasma expansion into the SOL area. Simple estimation, for example of the National Spherical Torus Experiment (NSTX) tokamak pedestal plasma conditions [6], i.e. for $n_e = 7 \times 10^{13}\,\mathrm{cm}^{-3}$, $T_e = 500\,\mathrm{eV}$ and $T_i = 750\,\mathrm{eV}$, showed that the time between scattering events [7] for ions is $\tau_i = 4 \times 10^{-4}\,\mathrm{s}$, and for electrons is $\tau_e = 4 \times 10^{-6}\,\mathrm{s}$. The predicted parameters for ITER pedestal plasma ($n_e = 3 \times 10^{13}\,\mathrm{cm}^{-3}$, $T_e = 1.7\,\mathrm{keV}$ and $T_i = 2.5\,\mathrm{keV}$ [8]) give even more pessimistic numbers that prevent the correct use of the Navier–Stokes equations: $\tau_i = 1 \times 10^{-2}\,\mathrm{s}$ and $\tau_e = 2 \times 10^{-4}\,\mathrm{s}$. The classical MHD approach assumes that the time between particles scattering is much smaller than duration of the simulated events (duration of the ELM time is about $\tau_{ELM} = 10^{-4}$–$10^{-3}\,\mathrm{s}$ [9]). However, as was shown in recent studies [2–4], implementation of various modifications and assumptions to the basic MHD system of equations allows one to calculate the parameters of the escaped core plasma particles close enough to the measured experimental data. The main problem lies in the fact that transport properties of the tokamak magnetized plasma cannot accurately be described with pure classical theory. The classical transport theory is valid for collisional plasma in a homogeneous and stationary magnetic field [10]. The classical theory should be expanded to include various turbulence mechanisms to explain the anomalous plasma transport properties in tokamaks [11].

The simulation results were significantly improved when the general SOL transport problem was divided into two subtasks: (1) MHD of the escaping core plasma, starting from the last closed flux surface (LCFS) and (2) MHD of the SOL neutrals (background gas) [3]. Solution of the first subtask for the escaping core plasma is used as a volume source for the neutral transport equations. This approach was used in a simplified NSTX geometry where the profiles of divertor heat and particle fluxes were calculated and compared with experimental data [12]. Recent investigations showed that splitting of the SOL transport problem and implementation of various hybrid approaches are prospective ways for better modelling of edge plasma evolution and correctly predicting component heat loads [13–16]. However, it should be stated that a full direct integrated model of the SOL plasma is still a very complex problem and only simplifications allow one to simulate characteristics of tokamak operation in a reasonable time.

Most recent experimental and theoretical studies of PFC erosion only considered plasma behaviour around local areas of the tokamak geometry [17–20]. Investigators have significant limitations in computational power and relevant experimental data due to design complexity, the numerous physical processes involved and difficulties in the integration of micro- and macro-scale processes. However, understanding various edge plasma processes and their interdependence in the entire SOL area are critically needed for accurate and reliable operation of future higher power devices. In our previous studies [18], we simulated the evolution of edge plasma during normal and disruptive operation only in localized areas of the SOL using the High Energy Interaction with General Heterogeneous Target Systems (HEIGHTS) computer simulation package with various integrated models [21–23]. These simulations showed a potential serious damage of nearby divertor surfaces in ITER-like devices during giant ELMs and disruption, not directly from the core plasma particles but from the high radiation fluxes of the evolving divertor plasma-shielding layer. We simulated in detail the energy load of core plasma particles deposited into component surface, heat conduction, melting and vapourization of the divertor material. The vapour MHD evolution and expansion was modelled including vapour heating by the incoming escaped core plasma particles and photon radiation generated within. Magnetic diffusion, heat conduction and radiation transport were also studied in the generated edge plasma. We concluded that the erosion of divertor surfaces is a complex self-consistent problem where the heat load to localized areas should be coupled through MHD and radiation transport processes of the evolving shielding cloud. Expansion of the computational domain to include the entire SOL area leads, however, to the necessary multiscale description of the complex reactor design that results in unavoidable extensive calculation time and the complex description of calculation domain. For example, the size of a typical fusion device is measured in metres, accurate MHD calculations require cell size of 100–200 μm, and detail surface erosion processes require a fine discretization level, with cell size less than 0.5–1.0 μm.

In this study, we introduce for the first time, a comprehensive kinetic Monte Carlo model for the simulation of the escaping core plasma and for the prediction of heat load to tokamak PFCs using the entire 3D device geometry. We implemented detail description of the escaping core particles into the SOL that will be used as volume source input in the HEIGHTS integrated models. This work includes (1) a model of the core particles escaping and a benchmark with available data and (2) simulation results that show details of the escaped particle drift separation and composition on inner and outer divertor surfaces. Based on the above-mentioned advantages of splitting the transport problem, our upgraded model includes both of the two separated subtasks. However, opposed to other existing models, we do not use any fitting parameters or averages from continuum media, i.e. we do not solve Navier–Stokes equations for the escaped core DT plasma. Similar to the UEDGE model [12], we separate the escaping core plasma particles and the edge plasma evolution; however, opposite to the UEDGE model we simulate the motion of the escaping core plasma as individual particles in the complex electromagnetic field structure of the device. The calculations presented below show the comparison between both models. However, the advantages of our approach are the ability to study various drift phenomena, to separately divide the contribution of ions and electrons into component heat loads and to exclude artificial fitting parameters usually used in the description of anomalous transport properties. The particle's motion is calculated using *ab initio* models with simulation of all possible scattering processes along their path. Results from our developed Monte Carlo kinetic model will then be used as an input volume source for the solution of the second subtask, i.e. MHD evolution of the edge plasma. It should be stated that the complete solution should include the edge plasma MHD 'feedback', i.e. SOL hydrodynamics will influence particles escaping, drift and scattering processes as well. Initially SOL is filled with near vacuum gas density. The scattering probability of the D, T and e in SOL is therefore small. As consequences

of plasma instabilities and interactions with divertor/wall, surface vaporization causes a density increase in SOL. As a result, the escaped core particles will undergo scatterings in SOL far from device walls. We are currently extending our models to two-component mixture plasma (DT + impurities) in the next HEIGHTS package upgrade. Future studies will treat SOL with real 'dirty' edge plasma, calculation of the thermodynamic properties of partially ionized plasma and simulation of radiation transport processes in mixed multi-component plasmas. The main goal of this study is to validate our approach of splitting the SOL transport problem and to assess the applicability of the developed kinetic Monte Carlo model for the calculation of the volume input source for the edge plasma MHD equations. We analysed and compared our simulation results with known experimental data.

2. Mathematical and physical models

As we discussed in our previous work [18], the edge plasma MHD equation system is described using the conservation laws of mass, momentum, energy and magnetic field as

$$\begin{aligned}
&\frac{\partial \rho}{\partial t} + \nabla \cdot (\rho \boldsymbol{v}) = Q_{\mathrm{m,vap}} \\
&\frac{\partial \rho \boldsymbol{v}}{\partial t} + \nabla \cdot \left(\rho \boldsymbol{v}\boldsymbol{v} + p_{\mathrm{t}} - \frac{\boldsymbol{B}\boldsymbol{B}}{4\pi\mu} \right) = -\frac{1}{4\pi\mu} \boldsymbol{B}(\nabla \cdot \boldsymbol{B}) \\
&\frac{\partial e_{\mathrm{t}}}{\partial t} + \nabla \cdot \left[\boldsymbol{v}(e_{\mathrm{t}} + p_{\mathrm{t}}) - \frac{1}{4\pi\mu}(\boldsymbol{v} \cdot \boldsymbol{B}) \cdot \boldsymbol{B} \right. \\
&\qquad \left. + \frac{c^2 \eta}{16\pi^2\mu^2} (\nabla \times \boldsymbol{B}) \times \boldsymbol{B} \right] \\
&\quad = Q_{\mathrm{th}} + Q_{\mathrm{rad}} + Q_{\mathrm{e,vap}} + Q_{\mathrm{imp}} - \frac{1}{4\pi\mu}(\boldsymbol{v} \cdot \boldsymbol{B})(\nabla \cdot \boldsymbol{B}) \\
&\frac{\partial \boldsymbol{B}}{\partial t} + \nabla \cdot (\boldsymbol{v}\boldsymbol{B} - \boldsymbol{B}\boldsymbol{v}) + \frac{c^2}{4\pi\mu} \nabla \times (\eta \nabla \times \boldsymbol{B}) = -\boldsymbol{v}(\nabla \cdot \boldsymbol{B}).
\end{aligned} \tag{1}$$

Here, ρ is the density; $\boldsymbol{v}$ is the velocity; $\boldsymbol{B}$ is the magnetic field; e_{t} is the total energy, which includes the hydrodynamic part, $e_{\mathrm{h}} = e_{\mathrm{in}} + e_{\mathrm{kin}}$ and the magnetic part $e_{\mathrm{m}} = (B^2/8\pi\mu)$; e_{in} is the internal energy; $e_{\mathrm{kin}} = (\rho v^2/2)$ is the kinetic energy. Analogous to energy, pressure has hydrodynamic and magnetic parts: $p_{\mathrm{t}} = p_{\mathrm{h}} + (B^2/8\pi\mu)$. Magnetic diffusion processes are taken into account as the Joule heating term, $(c^2\eta/16\pi^2\mu^2)(\nabla \times \boldsymbol{B}) \times \boldsymbol{B}$, in the total energy equation and as the diffusion term, $(c^2/4\pi\mu)\nabla \times (\eta \nabla \times \boldsymbol{B})$, in the magnetic field equation, where η is the resistivity, μ is the magnetic permeability and c is the light speed. In our calculations we assume $\mu = 1$ for the plasma. The thermal conduction in the plasma is included in the energy equation as the Q_{th} term. The target vapourization processes are taken into account as $Q_{\mathrm{m,vap}}$ and $Q_{\mathrm{e,vap}}$ sources in the continuity and energy equations, respectively. The Q_{rad} term describes the radiation transport processes. The external energy source Q_{imp} that takes into account the energy input from the escaped core particles into the edge plasma is the main theme of this study.

To avoid the limitations described above in edge plasma modelling and to preserve the multiscale approach in the integrated physical and mathematical models, we

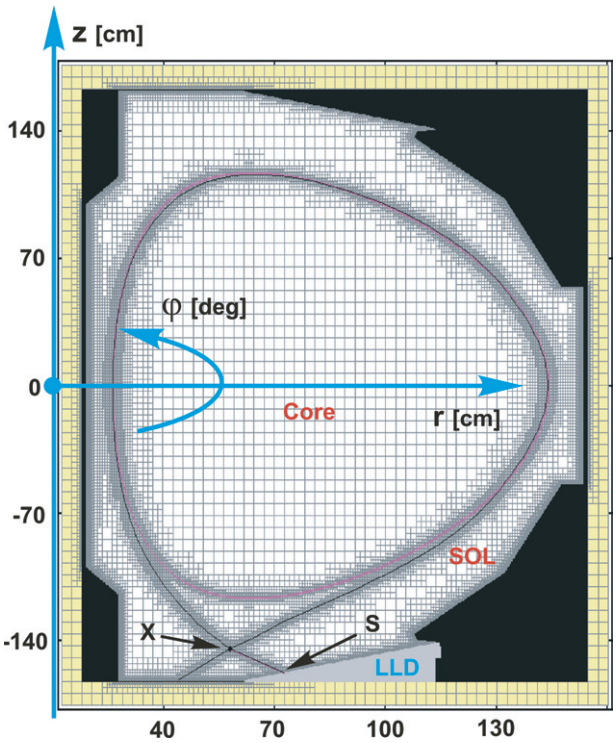

Figure 1. Schematic illustration of the quadtree meshe refinement model to describe NSTX geometry.

implemented the adaptive mesh refinement (AMR) algorithm with unstructured grid geometry [24] and upgraded all integrated routines in the HEIGHTS numerical package and computational algorithms for the AMR configuration. A five-layer quadtree method [25] is used for the AMR simulation of the entire SOL plasma evolution (figure 1). The AMR technique was integrated with our algorithms for the MPI parallel implementation of HEIGHTS.

The equilibrium plasma configuration used in our study for the initial conditions was extracted from the EQDSK database files [12, 26] and reconstructed for the quadtree mesh (figure 2). The magnetic field components were calculated from the stored poloidal fluxes as

$$B_r = \frac{1}{r}\frac{\partial \Psi}{\partial z}, \qquad B_\varphi = \frac{R_c B_c}{r}, \qquad B_z = -\frac{1}{r}\frac{\partial \Psi}{\partial r}. \tag{2}$$

Here, $B_{r,\varphi,z}$ is the magnetic field components in any point $P(r, \varphi, z)$; Ψ is the poloidal magnetic field and R_c, B_c are the radius and toroidal magnetic field at the tokamak magnetic centre.

The RBBBS and ZBBBS values stored in the standard G-EQDSK file[1] determine the tokamak core plasma border, i.e. the LCFS where we begin sampling the start point of the escaped core particles. HEIGHTS has the flexibility to describe the escaping particles from the LCFS using any spatial and temporal distribution to cover the possible wide range of escaping core plasma parameters during normal and disruptive operations. We can also use different initial temperatures of electron and ion compositions. In this study, we used equal probability distribution of the escaped particles along the entire LCFS and uniform temporal distribution of the impact

[1] https://fusion.gat.com/theory/Efitgeqdsk

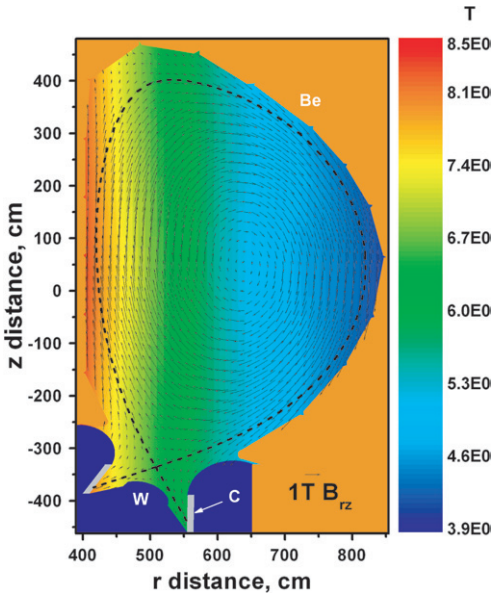

Figure 2. Initial magnetic field, separatrix and LCFS locations reconstructed from the EQDSK file (ITER design).

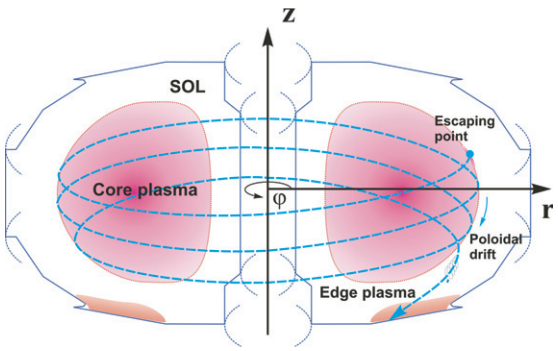

Figure 3. Schematic illustration of the escaped core particles in the 3D Monte Carlo package.

power deposition. The initial direction of the particles was sampled as 3D equiprobable so that electrons and ions can be returned to the core plasma or can move along the 'passed' or 'trapped' trajectory [27]. Figure 3 schematically illustrates our simulation of the escaped core particle motion implemented in HEIGHTS.

As illustrated in figure 3, particles are moving in a 3D cylindrical $S(r, \varphi, z)$ coordinate system where r is the radial, φ is the toroidal and z is the axial coordinate. This is the general system used in the HEIGHTS package. We do not use the MC method for the solution of the continuity equation. The escaped core media are not considered as continuous with pre-calculated or measured transport coefficients along and across the magnetic field. In our simulation, we considered real ions and electrons with Larmour gyration and toroidal motion within the complex structure of the magnetic field. However, equations of motion of charged particles in the arbitrary directed magnetic and electric fields are extremely awkward. We, therefore, introduced and expressed the equation of motion in the auxiliary Cartesian system $S'(x', y', z')$, where the z' axis is the direction parallel to the local magnetic field vector $\vec{B}$, i.e. in our virtual coordinate system S', there is only one magnetic field component $B'_z = |\vec{B}| = B$. This redefinition allows expressing the equation of motion in a compact form for the velocity components:

$$\begin{cases} V'_x = \left(V'_{0x} - \dfrac{cE'_y}{B}\right)\cos\left(\dfrac{qB}{m_r c}t\right) \\ \quad + \left(V'_{0y} - \dfrac{cE'_x}{B}\right)\sin\left(\dfrac{qB}{m_r c}t\right) + \dfrac{cE'_y}{B} \\ V'_y = \left(V'_{0x} - \dfrac{cE'_y}{B}\right)\sin\left(\dfrac{qB}{m_r c}t\right) \\ \quad + \left(V'_{0y} - \dfrac{cE'_x}{B}\right)\cos\left(\dfrac{qB}{m_r c}t\right) - \dfrac{cE'_x}{B} \\ V'_z = V'_{0z} + \dfrac{qE'_z}{m}t, \end{cases} \tag{3}$$

and for coordinates:

$$\begin{cases} x' = x'_0 + \dfrac{cE'_y}{B}t + \dfrac{m_r c}{qB}\left\{\left(V'_{0x} - \dfrac{cE'_y}{B}\right)\sin\left(\dfrac{qB}{m_r c}t\right)\right. \\ \quad \left. - \left(V'_{0y} + \dfrac{cE'_x}{B}\right)\cos\left(\dfrac{qB}{m_r c}t\right) + V'_{0y} + \dfrac{cE'_x}{B}\right\} \\ y' = y'_0 - \dfrac{cE'_x}{B}t + \dfrac{m_r c}{qB}\left\{\left(V'_{0x} - \dfrac{cE'_y}{B}\right)\cos\left(\dfrac{qB}{m_r c}t\right)\right. \\ \quad \left. + \left(V'_{0y} + \dfrac{cE'_x}{B}\right)\sin\left(\dfrac{qB}{m_r c}t\right) - V'_{0x} + \dfrac{cE'_y}{B}\right\} \\ z' = V'_{0z}t + \dfrac{qE'_z}{2m_r}t^2, \end{cases} \tag{4}$$

where $E'_{x,y,z}$ are the electric field components in the S' coordinate system; x'_0 and V'_0 are the initial location and velocity of particle; $m_r = m/\sqrt{1 - V^2/c^2}$ is the particle relativistic mass; t is the time; and c is the speed of light. Equations (3) and (4) are valid within one MHD cell border and one time step.

The transformation between the S and S' system can be expressed using the three Euler angles: φ_0, Φ and Θ [28], where φ_0 is the initial toroidal angle coordinate of the particle in the S system and the last two angles are determined from the local magnetic field as

$$\begin{aligned} \sin\Phi &= \frac{B_r\cos\varphi_0 + B_\varphi\sin\varphi_0}{|B_\varphi|}, \\ \cos\Phi &= \frac{B_r\sin\varphi_0 - B_\varphi\cos\varphi_0}{|B_\varphi|} \end{aligned} \tag{5}$$

and

$$\sin\Theta = \frac{|B_\varphi|}{B}, \qquad \cos\Theta = \frac{B_z}{B}. \tag{6}$$

After calculation of the transformation matrices $\boldsymbol{A}$ and $\boldsymbol{B}$:

$$\boldsymbol{A} = \begin{bmatrix} \cos\Phi & \sin\Phi & 0 \\ -\sin\Phi\cos\Theta & \cos\Phi\cos\Theta & \sin\Theta \\ \sin\Phi\sin\Theta & -\cos\Phi\sin\Theta & \cos\Theta \end{bmatrix},$$

$$\boldsymbol{B} = \begin{bmatrix} \cos\varphi_0 & -\sin\varphi_0 & 0 \\ \sin\varphi_0 & \cos\varphi_0 & 0 \\ 0 & 0 & 1 \end{bmatrix}, \tag{7}$$

an image of vector $\boldsymbol{V}(r, \varphi, z)$ in a virtual system can be calculated as $\boldsymbol{V}' = \boldsymbol{ABV}$. Since both the initial and virtual

systems are orthogonal, the reverse transformation can be calculated by simple matrix transpose $\boldsymbol{V} = \boldsymbol{B}^{\mathrm{T}}\boldsymbol{A}^{\mathrm{T}}\boldsymbol{V}'$.

The transport of individual particles in plasma is dominated by the long-range Coulomb force that results in a large number of small interactions. Since it is not feasible to simulate each interaction, a single-collision Monte Carlo approach to particle transport is not applicable for many situations of practical interest. Therefore, small interactions are lumped together and treated in a continuous manner. In the interactions of particles with walls, the energy losses are due to soft interactions with the target atomic electrons (excitation and ionization loss). The changes in the electron direction are mostly due to multiple Coulomb scattering from the nucleus, with some contribution from soft electron scattering [29]. Due to the limited computational power, it is difficult to take into account all interactions of the incident particles with target atoms. We divided these interactions into two groups: close collisions and distant collisions as is traditionally used in other Monte Carlo codes. The criterion for grouping is the energy that is transmitted to the recoiled particle. Since most of the distant interactions do not have a critical effect on the incident particle energy or direction of motion, they can be considered as the combined contribution of small interactions and their common effect can be comparable to the interaction of close scattering events, depending on the incident initial energy. In our model, all interactions where incident particles lose <1% of their initial energy are considered as distant. The distant interaction contribution (energy and direction change) is accumulated along the trajectory between two close collisions and is added at the end of the trajectory. This approach is applied to the simulation of all scattering processes in the SOL and to tokamak component surfaces. Various physical processes include ion–nuclear, ion–electron, electron–nuclear, electron–electron interactions, the bremsstrahlung process, photoabsorption, the Compton process and Auger relaxation. The algorithm takes into account contribution of the secondary (recoiled) particles, if their energy is higher than a critical value. HEIGHTS models of plasma particle interaction with matter are described in detail in [21, 29, 30]. The new 3D Monte Carlo algorithm is developed and benchmarked for plasma particle interactions with solid and plasma matter in the magnetic field for any geometrical configuration.

3. Validation and benchmarking

The procedure of benchmarking HEIGHTS models and computer package includes both individual validations of separate blocks and components as well as benchmarking the whole integrated package against available experimental and theoretical data. In this study we present benchmarking results and comparisons that verify our new kinetic model for the evolution of the escaping core particles. To further demonstrate the applicability of our approach we performed benchmark simulations for two different magnetic configurations, i.e. NSTX and ITER design. We simulated particle flow evolution during both normal and disruptive operations of plasma. Heat flux distribution on the divertor plate surface was the parameter used for comparison of results.

The NSTX ($R = 0.85\,\mathrm{m}$, $a < 0.67\,\mathrm{m}$, $R/a > 1.27$) experimental and simulation data [12] was used to validate our model in low-field devices. We used the published NSTX discharge parameters for the initial conditions in our developed kinetic model. The temperatures used for the escaped core electrons and ions were $T_\mathrm{e} = 130\,\mathrm{eV}$, $T_\mathrm{i} \sim T_\mathrm{e} - 15\,\mathrm{eV}$. The incident power was estimated to be $P_\mathrm{imp} = 1.75\,\mathrm{MW}$. The starting points of outgoing/escaping particles from the core were assumed equally distributed around the LCFS and initial particle velocity was directed in the 3D space with equal probability. Figure 4 shows the simulated heat flux distribution on the divertor surface from our kinetic model in comparison with the heat flux measured in the NSTX experiment as well as calculated by the UEDGE code [12]. Since HEIGHTS currently calculates unperturbed escaped core particles, the flux distribution has a slightly narrower footprint in comparison with the experimental results. When taking into account edge plasma evolution with impurity content, which is not correctly treated in most previous simulations, it will result in broader particle/heat flux distributions and to the reduction of peaks. However, correct peak location, compliance of curves form and total energy demonstrate good agreement between our calculations and the published experimental data.

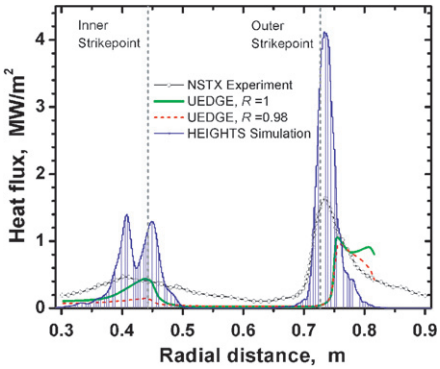

Figure 4. Comparison of HEIGHTS calculated heat flux at the NSTX divertor surface with experimental data and other simulations.

The second benchmark for model validation was performed for ITER geometry and magnetic field configurations. To confirm our previous calculations performed using localized geometry simulation [18], we compared the disruption spatial power density footprints on the outer divertor surface. The initial conditions for disruption parameters in our simulations assumed a total energy of the escaped particles $Q = 126\,\mathrm{MJ}$, impact duration $\tau = 1\,\mathrm{ms}$ and particles temperature $T = 3.5\,\mathrm{keV}$. In previous calculations, the computational domain was limited for the divertor nearby area; and the estimated spatial distribution [23] of disruption particles was sampled directly on the domain border. In our new model, the final spatial distribution is the result of the integrated approach of the entire 3D SOL reactor geometry. A reasonable agreement between the two different models is illustrated in figure 5.

4. Simulation results

A full 3D kinetic description of the escaping core particles is required to realistically study particle evolution in the complex magnetic configurations and geometries of current and future tokomaks. We should stress that the presence of strong

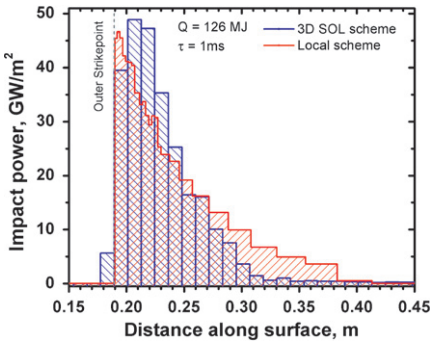

Figure 5. Comparison of HEIGHTS 3D kinetic model with previous localized model [18] calculations of the heat flux during disruption on the ITER outer divertor surface.

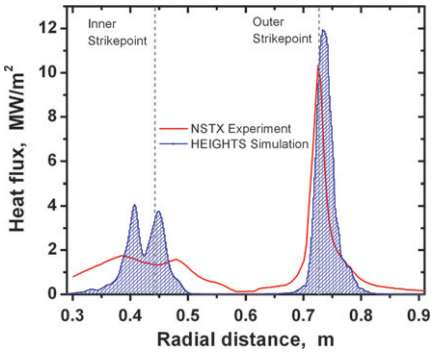

Figure 6. Heat flux footprint at the NSTX divertor surface. Power shot $P_{NBI} = 4.9$ MW.

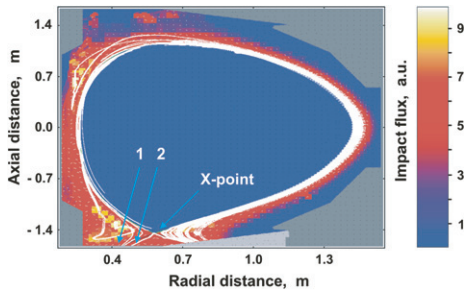

Figure 7. Poloidal cross-section of the impact particle flux in NSTX: white lines show particle trajectories; arrows 1 and 2 show the location of heat load peaks at the inner divertor.

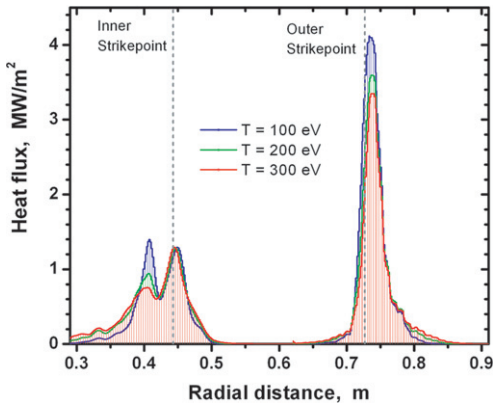

Figure 8. Dependence of NSTX divertor heat flux footprints on the escaped core particle initial temperature.

spatial effects cannot be described with simple and lower dimensional models. The complex feature of the magnetic field-induced plasma drift in SOL and divertor nearby areas is the starting point to determine the hydrodynamics evolution and radiation phenomena at the surface of PFCs. First, we studied the initial dependences that determine the heat load conditions at the divertor surface. Based on our simulations, we should point out that the typical ratio of the outer to inner divertor peak heat flux is based on the stochastic character of the escaping core particles in current device magnetic field configuration. Our detailed results of the ratio of inner and outer flux distributions agree with the commonly observed behaviour in several tokamaks. Figure 6 shows HEIGHTS calculations of the NSTX power discharge [31]. The initial particle temperature was not discussed in [31]; however, as we will show later that this parameter does not significantly affect the results. The flowing particle power was estimated from the neutral beam injection power $P_{NBI} = 4.9$ MW [12].

As is shown in figure 6, the heat flux profile on the inner divertor surface has two peaks. The experimental results shown for NSTX indicate that the additional peak appears when the shot power is increased. Our modelling results, for the first time, show similar two-peak formation and to explain this effect we tracked individual particles that formed the second peak. Examples of the escaped core particle trajectories are shown in figure 7 with white lines having the highest impact flux. Arrow 2 shows the second peak location. This location is the arrival spot and concentration of the particles departed from the X-point region. Comparison of figures 4 and 7 brings to a conclusion that peak #2 exists originally, i.e. this main source of heat flux on the inner divertor is due to the 'leakage' from the X-point area. Therefore, we can define the trajectories and the drift processes from the tokamak high-field side as #1 and from the X-point area as #2. The direct impact of process #1 is negligible because of particles returning to core plasma (see trajectories in figure 7). Increasing the discharge power stimulates and enhances process #1 corresponding to the experimental data [31].

However, this process cannot be simply explained by changing the temperature of escaping plasma with increasing discharge power. We simulated the escaping core plasma particles with various initial temperatures in the NSTX and ITER magnetic configuration. Figure 8 shows interesting results that increasing the initial temperature of the escaping particles tends to decrease the particle flux in trajectories #1. Moreover, it also tends to increase the probability of particles returning to the core on the low-field side and to the slight decrease in the outer divertor flux.

Figure 9 demonstrates an opposite behaviour of the dependence of the escaped core particles on the initial temperature in a similar analysis but for ITER geometry and magnetic configuration. An increase in the initial temperature of the escaped core particles tends to slightly increase the divertor heat flux.

Both figures 8 and 9 indicate that the initial temperature of the escaped particles does not directly play a major role in the magnitude of the divertor heat flux (in the reasonable limits of used temperature values). The magnetic field configuration and the generated radial electric field are the main parameters

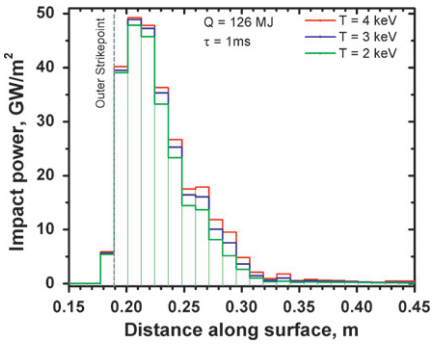

Figure 9. Dependence of ITER outer divertor heat flux on the initial temperature of the escaped core particles.

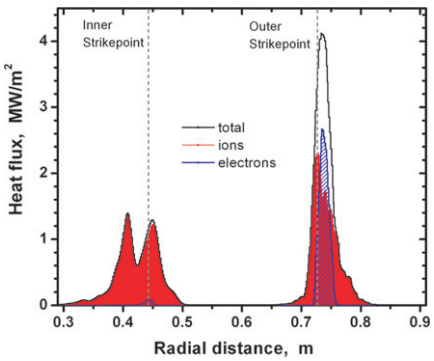

Figure 10. Input of electrons and ions energy to the heat load on NSTX divertor surface.

that determine core particle input into the SOL area. The effect of the radial electric field on the escaping core particles is currently under investigation.

The drift of the charged particles due to the gradient of the magnetic field has an opposite direction for ions and electrons. The large mass difference between these particles and the resulting Larmour radii inequality makes the escaping probability of core plasma different for electrons and for ions. The radial electric field appears due to charged particle separation around the LCFS. The generated electric field cannot totally compensate for the charged particle separation because of the presence of the magnetic field. This is clear from the analysis of equations (3) and (4) where the last right term of these equations has only E/B expressions and does not include q in the poloidal plane. Exception is given only for the z' direction that was chosen to be parallel to the local magnetic field, i.e. compensation is effective only in the tokamak toroidal direction. In the poloidal direction, the charged particles can drift uncompensated and the final divertor heat distribution is composed of the separate flows of electrons and ions [32]. This results in the shaping of the energy deposition profile along the divertor surface and in depth because of the deeper electron penetration and the biasing in the SOL and on PFCs [33, 34]. Figure 10 shows the spatial distribution of the heat flux on NSTX divertor surface where the input of the electrons and ions are shown separately. As is shown, the inner divertor heat load is formed mainly due to energy deposition of the ions.

The flux shapes presented above are for the case of no divertor plasma. These results are of obvious importance

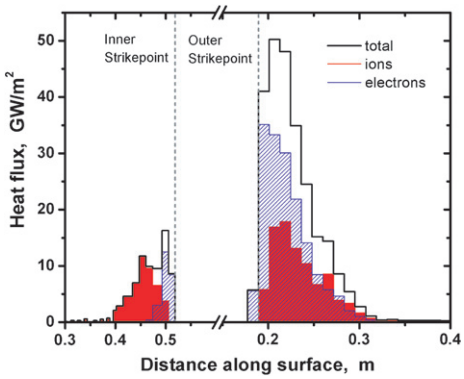

Figure 11. Contributions of electron and ion energy to heat load on the ITER divertor surface.

as initial conditions for modelling edge plasma phenomena and for PFC damage and possible mitigation techniques. Information about separate contributions of the divertor heat flux due to ions and electrons is very limited in spite on the fact that electrons and ions play very different roles in the undersurface processes. Figure 11 shows prediction of the heat load composition for the ITER divertor surfaces. As shown previously in figure 10, the electron flux is concentrated at the strike points but opposite to the NSTX case, i.e. the electron part is much larger in the ITER case. Our simulations (figures 8 and 9) indicated the weak dependence of the heat flux spatial profile on the initial particle temperature and we are currently analysing the heat flux dependence on the magnetic field configuration.

5. Conclusions

We have developed multidimensional comprehensive models for extensive and integrated simulation of the escaped core plasma impact on the tokamak divertor and nearby locations. The 3D kinetic Monte Carlo model of the escaping core particles is developed for the self-consistent analysis of the MHD evolution of the initiated edge plasma where the escaping particles are used as the input volume source. The escaped plasma part simulates particle evolution (motion and scatterings) in full 3D in the presence of local magnetic and electric fields starting from the LCFS through the entire SOL area and up to penetration inside tokamak components. The quadtree adaptive mesh refinement algorithms with 5 level sublayers were developed and implemented in HEIGHTS to significantly enhance the accuracy of the calculation and to reduce the computational time. We implemented, verified and benchmarked our new Monte Carlo kinetic model in our HEIGHTS simulation package to study the spatial profile of ion and electron energy deposition of the escaped core particles of both inner and outer divertor plates for NSTX and ITER device parameters, magnetic field complex structure and the components' geometry. We also studied the influence of initial temperature of the core escaping particle on the divertor heat load footprints. For accurate prediction of the actual divertor damage and to gain more physical insights of various processes we calculated, for the first time, details of the electron–ion composition and contribution to the surface heat fluxes at both the inner and outer divertor plates. The distribution profile

was in good agreement with available data and explained the different contributions and sources among ions and electrons and their dependences on machine parameters.

Acknowledgment

This work is supplied by the US Department of Energy, Office of Fusion Energy Sciences.

References

[1] Kulsrud R.M. 1983 MHD description of plasma *Handbook of Plasma Physics* vol 1 *Basic Plasma Physics* ed M.N. Rosenbluth and R.Z. Sagdeev (Amsterdam: North-Holland)
[2] Hu Q. *et al* 2012 *Nucl. Fusion* **52** 083011
[3] Lore J.D. *et al* 2012 *Nucl. Fusion* **52** 054012
[4] Militello F. *et al* 2012 *Plasma Phys. Control. Fusion* **54** 095011
[5] Paccagnella R. *et al* 2009 *Nucl. Fusion* **49** 035003
[6] Kugel H.W. *et al* 2011 *J. Nucl. Mater.* **415** S400
[7] Braginskii S.I. 1965 Transport processes in a plasma *Reviews of Plasma Physics* vol 1, ed M.A. Leontovich (New York: Consultants Bureau)
[8] Erents S.K. *et al* 2007 *J. Nucl. Mater.* **363–365** 565
[9] Loarte A. *et al* 2007 *Nucl. Fusion* **47** S203
[10] Shaing K.C. 1997 *Phys. Plasmas* **4** 3320
[11] Angioni C. *et al* 2009 *Plasma Phys. Control. Fusion* **51** 124017
[12] Stotler D.P. *et al* 2010 *Contrib. Plasma Phys.* **50** 368
[13] Todo Y. *et al* 2012 *Nucl. Fusion* **52** 033003
[14] Budny R.V. *et al* 2012 *Nucl. Fusion* **52** 023023
[15] Frerichs H. *et al* 2012 *Nucl. Fusion* **52** 023001
[16] Kritz A.H. *et al* 2011 *Nucl. Fusion* **51** 123009
[17] Coenen J.W. *et al* 2011 *Nucl. Fusion* **51** 083008
[18] Sizyuk V. and Hassanein A. 2010 *Nucl. Fusion* **50** 115004
[19] Gray T.K. *et al* 2011 *J. Nucl. Mater.* **415** S360
[20] Kreter A. *et al* 2009 *J. Nucl. Mater.* **390–391** 38
[21] Sizyuk V. and Hassanein A. 2009 *Nucl. Fusion* **49** 095003
[22] Hassanein A., Morozov V., Tolkach V., Sizyuk V. and Konkashbaev I. 2003 *Fusion Eng. Des.* **69** 781
[23] Hassanein A. and Konkashbaev I. 2003 *J. Nucl. Mater.* **313–316** 664
[24] Samtaney R. *et al* 2004 *Comput. Phys. Commun.* **164** 220
[25] Lee W., Borthwick A. and Taylor P., 2011 *J. Comput. Phys.* **230** 4848
[26] Rognlien T.D. *et al* 2007 *J. Nucl. Mater.* **363–365** 658
[27] Boyd T.J.M. and Sanderson J.J. 2003 *The Physics of Plasmas* (Cambridge: Cambridge University Press) p 33
[28] Krey U. and Owen A. 2007 *Basic Theoretical Physics* (Berlin: Springer) p 81
[29] Sizyuk V., Hassanein A. and Bakshi V. 2007 *J. Micro/Nanolith. MEMS MOEMS* **6** 043003
[30] Hassanein A., Sizyuk V., Sizyuk T. and Morozov V. 2007 *Proc. SPIE* **6517** 65171X
[31] Mastrovito D. *et al* 2003 *Rev. Sci. Instrum.* **74** 5090
[32] Federici G. *et al* 2003 *J. Nucl. Mater.* **313–316** 11
[33] Groth M. *et al* 2009 *Nucl. Fusion* **49** 115002
[34] Zweben S.J. *et al* 2009 *J. Nucl. Mater.* **390–391** 417